

PROCEEDINGS OF SPIE

[SPIDigitalLibrary.org/conference-proceedings-of-spie](https://spiedigitallibrary.org/conference-proceedings-of-spie)

3D wide field-of-view Gabor-domain optical coherence microscopy advancing real-time in-vivo imaging and metrology

Cristina Canavesi, Andrea Cogliati, Adam Hayes, Patrice Tankam, Anand Santhanam, et al.

Cristina Canavesi, Andrea Cogliati, Adam Hayes, Patrice Tankam, Anand Santhanam, Jannick P. Rolland, "3D wide field-of-view Gabor-domain optical coherence microscopy advancing real-time in-vivo imaging and metrology," Proc. SPIE 10053, Optical Coherence Tomography and Coherence Domain Optical Methods in Biomedicine XXI, 100530Z (17 February 2017); doi: 10.1117/12.2252187

SPIE.

Event: SPIE BiOS, 2017, San Francisco, California, United States

3D wide field-of-view Gabor-domain optical coherence microscopy advancing real-time in-vivo imaging and metrology

Cristina Canavesi^a, Andrea Cogliati^{a,b}, Adam Hayes^c, Patrice Tankam^c, Anand Santhanam^d, and Jannick P. Rolland^{a,c}

^aLighTopTech Corp., 150 Lucius Gordon Drive, Suite 201, West Henrietta, NY, USA 14586-9687;

^bDepartment of Electrical and Computer Engineering, University of Rochester, Rochester, NY, USA 14627; ^cThe Institute of Optics, University of Rochester, Rochester, NY, USA 14627; ^dUniversity of California Los Angeles, Department of Radiation Oncology, 200 Medical Plaza Dr., Los Angeles, CA USA 90095

ABSTRACT

Real-time volumetric high-definition wide-field-of-view in-vivo cellular imaging requires micron-scale resolution in 3D. Compactness of the handheld device and distortion-free images with cellular resolution are also critically required for on-site use in clinical applications. By integrating a custom liquid lens-based microscope and a dual-axis MEMS scanner in a compact handheld probe, Gabor-domain optical coherence microscopy (GD-OCM) breaks the lateral resolution limit of optical coherence tomography through depth, overcoming the tradeoff between numerical aperture and depth of focus, enabling advances in biotechnology. Furthermore, distortion-free imaging with no post-processing is achieved with a compact, lightweight handheld MEMS scanner that obtained a 12-fold reduction in volume and 17-fold reduction in weight over a previous dual-mirror galvanometer-based scanner. Approaching the holy grail of medical imaging – noninvasive real-time imaging with histologic resolution – GD-OCM demonstrates invariant resolution of 2 μm throughout a volume of $1 \times 1 \times 0.6 \text{ mm}^3$, acquired and visualized in less than 2 minutes with parallel processing on graphics processing units. Results on the metrology of manufactured materials and imaging of human tissue with GD-OCM are presented.

Keywords: nondestructive imaging, MEMS, Gabor-domain optical coherence microscopy, optical coherence tomography

1. INTRODUCTION

In-vivo imaging requires micrometer-scale resolution in 3D, depth of imaging at least of the order of 1 mm, and large field-of-view ($\geq 1 \text{ mm}$). In order to meet the requirements of real-time volumetric wide field-of-view imaging with histologic resolution for clinical applications, several state-of-the-art technologies are integrated in a high-definition, real-time, portable and robust instrument for on-site imaging.

2. GABOR-DOMAIN OPTICAL COHERENCE MICROSCOPY

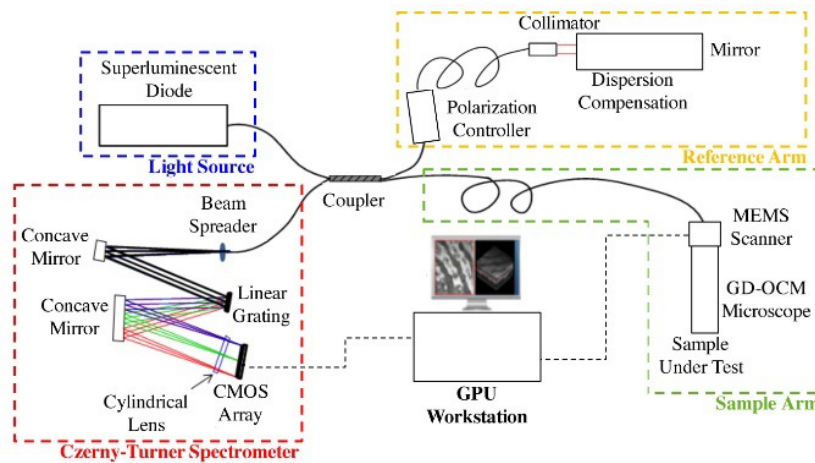
Gabor-domain optical coherence microscopy (GD-OCM) is a high-definition, noninvasive imaging technique based on Fourier-domain optical coherence tomography¹⁻³. The instrument is fiber-based and has a modular design. A schematic representation of the modules comprising a GD-OCM instrument is shown in Fig. 1(a). The broadband source is a superluminescent diode centered at 840 nm with 100 nm bandwidth. A custom spectrometer is used for the detection, enabling an imaging depth greater than 2 mm. A compact 2D MEMS scanner is integrated with a handheld probe housing a dynamic focusing microscope (Fig. 1(b)) for wide field-of-view cellular imaging⁴. A graphics processing unit (GPU) workstation is employed for fast processing and visualization of the 3D image⁵.

2.1 Wide field of view

A custom microscope was designed to achieve a lateral resolution of 2 μm over a large field of view of $1 \text{ mm} \times 1 \text{ mm}$. The lateral resolution is inversely proportional to the numerical aperture of the optical system, while the depth of focus is inversely proportional to the square of the numerical aperture of the system. Therefore, there is a fundamental tradeoff between lateral resolution and depth of focus; when increasing the numerical aperture of the optical system to achieve a 2 μm lateral resolution, as needed to resolve individual cells in human tissue, the depth of focus becomes significantly

*cristina@lightoptech.com; phone 1 585 484 0808; lightoptech.com

shallower ($<100\ \mu\text{m}$) than the millimeter scale imaging depth requirement for cellular imaging. In GD-OCM, in order to effectively extend the depth-of-focus and maintain a $2\ \mu\text{m}$ lateral resolution, a bio-inspired liquid lens is used to dynamically refocus the microscope through the sample depth with no moving parts. Multiple volumes with different in-focus regions are acquired and fused together with a method called Gabor fusing to produce a 3D image that has a resolution of $2\ \mu\text{m}$ in all dimensions^{2,6}.



(a)



(b)

Figure 1. (a) Schematic of the GD-OCM instrument, which is fiber-based and has a modular configuration. GPU: graphics processing unit; CMOS: complementary metal oxide semiconductor; MEMS: microelectromechanical systems; GD-OCM: Gabor-domain optical coherence microscopy. (b) Handheld operation is permitted by the lightweight probe integrating the GD-OCM microscope and MEMS scanner. A mechanical arm can also be used to avoid or mitigate artifacts due to possible operator hand motion.

2.2 Handheld probe

A handheld probe was developed for the MEMS scanner and integrated with the GD-OCM microscope (Fig. 1(b)), achieving a 12-fold volume reduction and a 17-fold weight reduction of the scanner over a previous galvanometer-based scanner, as shown in Fig. 2. The resulting GD-OCM instrument is portable and robust, and primed to be used on site in clinical or industrial settings.

The scanner is used to scan over an area of $1\ \text{mm} \times 1\ \text{mm}$; since the optical resolution is $2\ \mu\text{m}$, the imaging is performed at a sampling of $1\ \mu\text{m}$ (1000×1000 points over the field of view). A fast-axis scan of $57\ \text{Hz}$ was achieved, with a corresponding $57\ \text{kHz}$ A-scan acquisition rate.

A mechanical arm was also integrated in the system to house the handheld probe (Fig. 1(b)). The arm can be used in certain applications to avoid or mitigate artifacts due to operator movement.

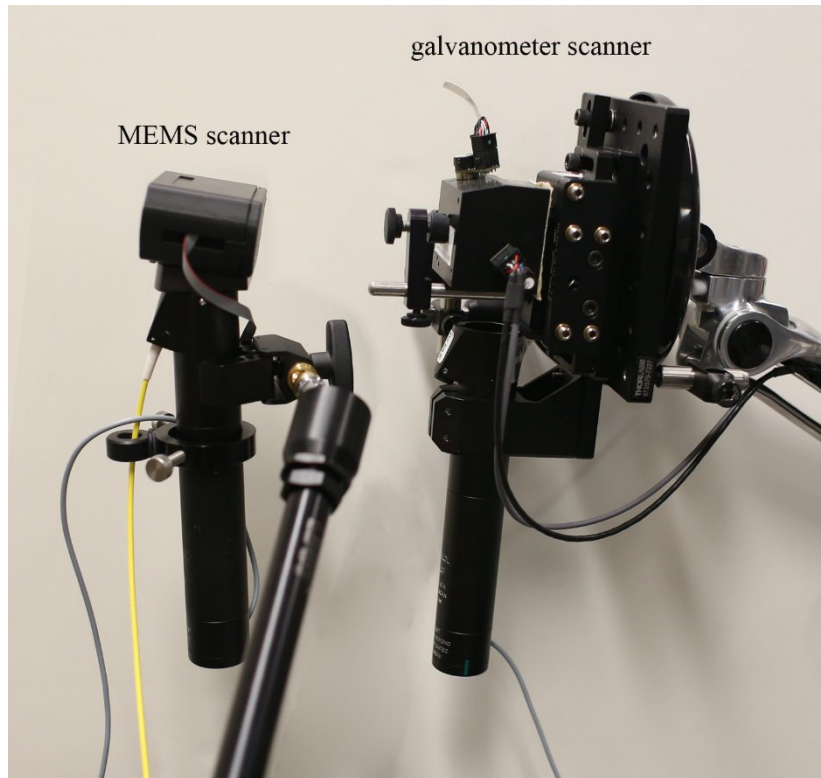


Figure 2. GD-OCM microscope and integrated scanner (left: MEMS-based; right: galvanometer-based). A 12-fold volume reduction and a 17-fold weight reduction were achieved with a MEMS scanner over the previous galvanometer scanner.

2.3 Distortion-free imaging

Distortion-free imaging with no post-processing is obtained by combining the custom microscope with a 2D MEMS scanner driven with a pre-shaped input signal⁴. This driving scheme is necessary due to the resonant nature of MEMS scanners; a linear signal in fact excites the resonant frequency of the MEMS, introducing oscillations, as shown in Fig. 3(a), that produce severe distortion of the image, as shown in Fig. 3(b), where the image of a regular microscopic structure is affected by gross distortions. The pre-shaped input signal avoids excitation of the MEMS resonance, as shown in Fig. 3(c), and produces undistorted images, retaining the sharp features of the microscopic structure, as shown in Fig. 3(d). The MEMS-based scanner produces 2D scanning of the sample over an area of $1 \text{ mm} \times 1 \text{ mm}$, and enables undistorted 3D imaging with no post-processing.

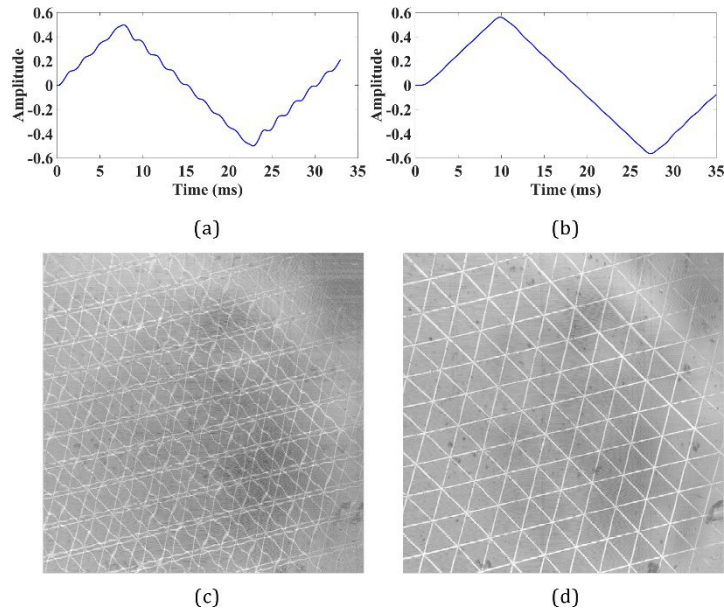


Figure 3. Distortion-free imaging is achieved with input shaping of the MEMS driving signal to avoid excitation of the resonance. The normalized angular movement of the MEMS is shown for a linear input and for a pre-shaped input in (a) and (b), respectively. The oscillations in (a), due to excitation of the resonant frequency of the MEMS, are avoided in (b). (c) and (d) show an *en face* view of a microscopic structure acquired with the MEMS driven with a linear signal and with the pre-shaped input driving the MEMS, respectively. In (c), the oscillations of the MEMS cause distortion over the entire field of view of the image, while in (d), the sharp features of the microstructure are preserved. The field of view is 1 mm \times 1 mm.

2.4 Real-time processing

Due to the large size of the acquired 3D images (1 μ m sampling over 1 mm \times 1 mm field of view), and the need to acquire, process and combine multiple volumes with different in-focus regions to achieve invariant cellular imaging through the volume of interest, the computation requirements for fast processing and visualization of GD-OCM images are quite demanding. A parallelized multi-graphics processing unit (GPU) framework is used to process the acquired volumes with different in-focus regions and combine them in the final 3D image⁵. Each volume is processed while the next volume is being acquired, for fast visualization of the final image. Figure 4 shows a schematic representation of the computation steps, which were implemented on Titan X GPUs (NVIDIA®).

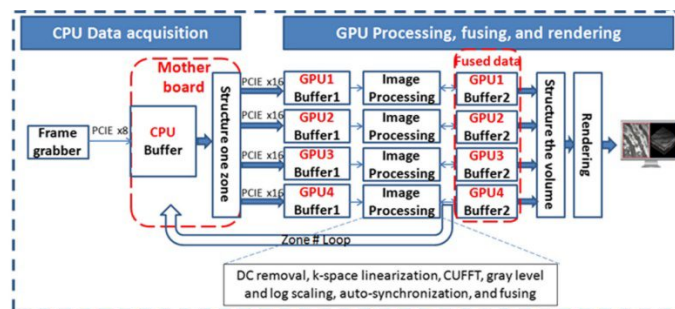


Figure 4. Multi-GPU architecture for GD-OCM image processing and visualization.

3. APPLICATIONS

The GD-OCM instrument was used to image human skin *in vivo* and excised human corneas, as shown in Figs. 5 and 6, respectively. Cellular resolution was achieved⁷.

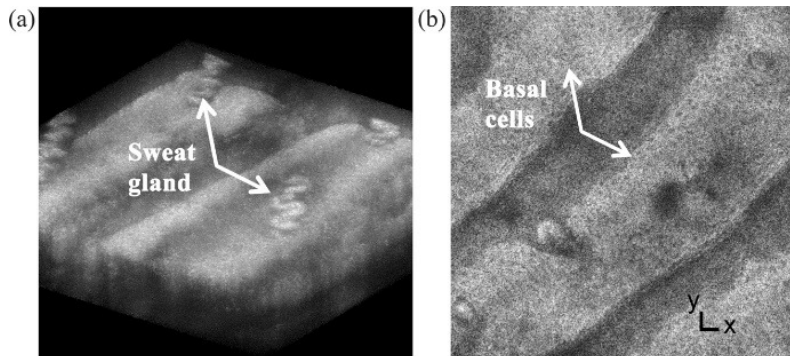


Figure 5. (a) 3D view of a human fingertip *in vivo*. Basal cells are visible in the *en face* image (b). The field of view is $1\text{ mm} \times 1\text{ mm}$.

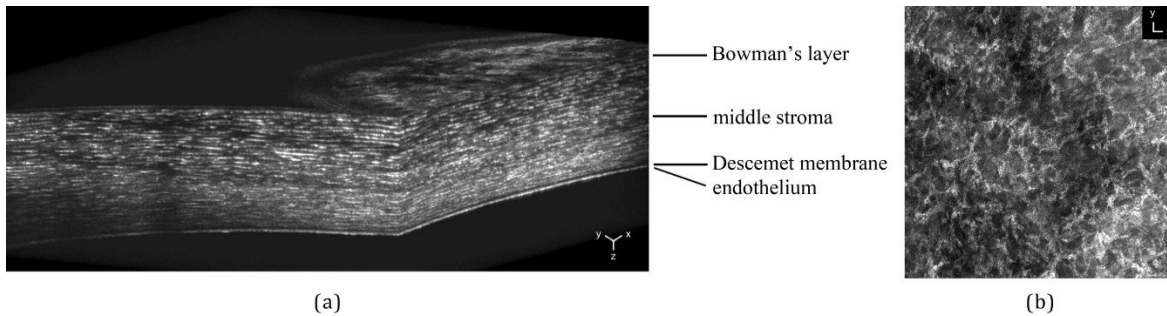


Figure 6. (a) 3D view of an excised human cornea. The field of view is $1\text{ mm} \times 1\text{ mm}$. Stromal keratocytes are visible in the XY *en face* image (b) of the middle stroma.

In addition to medical imaging, industrial applications also benefit from robust, fast high-resolution nondestructive imaging for metrology and quality control in manufacturing, such as contact lens manufacturing⁸.

4. CONCLUSION

High-definition, wide field-of-view imaging is achieved with a Gabor-domain optical coherence microscope with a MEMS-based handheld scanner and GPU processing. Through the integration of several state-of-the-art technologies, a compact, robust instrument was obtained. The instrument was tested in a clinical setting for 3D noninvasive imaging, achieving cellular resolution *in vivo*.

ACKNOWLEDGMENTS

This material is based upon work supported by the National Science Foundation under Grants No. IIP-1346453 and IIP-1534701, and by the NYSTAR Foundation and the Center for Emerging and Innovative Sciences. We thank NVIDIA® for the donation of GeForce® GTX Titan GPUs.

REFERENCES

- [1] A. F. Fercher, C. K. Hitzenberger, G. Kamp, and S. Y. El-Zaiat, "Measurement of intraocular distances by backscattering spectral interferometry," *Optics Communications*, 117, 43-48 (1995).
- [2] S. Murali, K. P. Thompson, and J. P. Rolland, "Three-dimensional adaptive microscopy using embedded liquid lens," *Optics Letters*, 34(2), 145-147 (2009).
- [3] J. P. Rolland, P. Meemon, S. Murali, K. P. Thompson, and K.-s. Lee, "Gabor-based fusion technique for Optical Coherence Microscopy," *Optics Express*, 18(4), 3632-3642 (2010).
- [4] A. Cogliati, C. Canavesi, A. Hayes, P. Tankam, V.-F. Duma, A. Santhanam, et al., "MEMS-based handheld scanning probe with pre-shaped input signals for distortion-free images in Gabor-Domain Optical Coherence Microscopy," *Optics Express*, 24(12), 13365-13374 (2016).
- [5] P. Tankam, A. P. Santhanam, K.-S. Lee, J. Won, C. Canavesi, and J. P. Rolland, "Parallelized multi-graphics processing unit framework for high-speed Gabor-domain optical coherence microscopy," *Journal of Biomedical Optics*, 19(7), 071410 (2014).
- [6] P. Meemon, J. Widjaja, and J.P. Rolland "Spectral fusing Gabor domain optical coherence tomography," *Optics Letters* 41(3), 508-512 (2016).
- [7] P. Tankam, Z. He, Y.-J. Chu, J. Won, C. Canavesi, T. Lepine, et al., "Assessing microstructures of the cornea with Gabor-domain optical coherence microscopy: pathway for corneal physiology and diseases," *Optics Letters*, 40(6), 1113-1116 (2015).
- [8] P. Tankam, J. Won, C. Canavesi, I. Cox, and J. P. Rolland, "Optical Assessment of Soft Contact Lens Edge-Thickness," *Optometry & Vision Science* 93(6), 987-996 (2016).